Journal of Non-Crystalline Solids xxx (2009) xxx–xxx

Contents lists available at ScienceDirect

Journal of Non-Crystalline Solids

journal homepage: www.elsevier.com/locate/jnoncrysol

Effect of synthesis conditions on the fractal structure of yttrium-stabilized zirconium dioxide

K.V. Kravchyk [a,*], Yu.P. Gomza [b], O.V. Pashkova [a], O.I. V'yunov [a], S.D. Nesin [b], A.G. Belous [a]

[a] V.I. Vernadskii Institute of General and Inorganic Chemistry, Palladina Avenue 32/34, 03680 Kyiv – 142, Ukraine
[b] Institute of Chemistry of High-Molecular Compounds, National Academy of Sciences of Ukraine, Khar'kovskoe sh. 48, Kiev 02610, Ukraine

ARTICLE INFO

Article history:
Received 4 October 2008
Received in revised form 11 September 2009
Available online xxxx

PACS:
81.07.Bc
81.16.Be
61.43.Hv

Keywords:
Ceramics
Nanoparticles
X-ray diffraction

ABSTRACT

The effect of synthesis conditions (sequential precipitation, coprecipitation, and sol–gel method) on the fractal structure of yttrium-stabilized zirconium dioxide has been investigated. It has been shown that the difference between methods manifests itself clearly in xerogel nanostructures, viz. by the number of fractal aggregation levels (three levels in hydroxide precipitates and two in sol–gel) and the absence of mass-fractal aggregation in sol–gel. It is been determined that the mass-fractal aggregation of precursors contributes to good filtration of hydroxide precipitates and allows preparation of oxides with soft, readily destructible aggregates, and that surface-fractal aggregation makes for good pressability of oxides.

1. Introduction

Yttrium-stabilized zirconium dioxide is of great practical importance since promising materials for structural ceramics [1] and solid electrolytes with oxygen ion conduction [2–4] are developed on its basis. The research carried out in recent years showed that materials of the new generation can be obtained on the basis of nanoscale precursors. It is known that nanoscale dispersions are inclined to self-assembly of particles into ordered structures [5,6]. In this case, structure hierarchy from primary clusters to conglomerate is formed [7].

In resent years, the concept of fractal aggregation, which is based on self-similarity principle, has been used to study materials with irregular structure [8,9]. Many synthesis products of precursors of new materials prepared under mild conditions (method of precipitation of slightly soluble compounds, sol–gel technology, etc.) may be objects with fractal aggregates. A great numeral of papers are devoted to the study of the fractal aggregation of various materials [10–18], the information on the fractal of ZrO_2-based materials being very scanty [16–18].

The fractal aggregation processes depend on the precursor preparation conditions and play a very important role in the material preparation process [5,6]. The simplest, cheapest and most ecologically pure precursor of stabilized zirconium dioxide, which is widely used for the manufacture of ZrO_2 ceramics, is a system of zirconium and yttrium hydroxides. Hydroxide precursors are generally prepared by the coprecipitation method. However, coprecipitated precipitates are poorly filterable and form after drying and calcinations very strong aggregates, which require long grinding. Changing precipitation conditions (hydroxide precipitation sequence, pH values) leads in a certain pH range to a considerable improvement of the filterability of precipitates and makes for obtaining stabilized nanoscale zirconium dioxide with weak bonds between particles (with the effect friability of aggregates of particles). In recent years, the interest in the preparation of nanoscale ZrO_2 by sol–gel method has increased.

The study of the effect of various above synthesis method on the fractal structure of ZrO_2-based dispersion is of interest. Therefore, the aim of the work is to study the effect of preparation conditions on the fractal structure of precursors and solid solutions of ZrO_2–Y_2O_3 oxides.

2. Experimental

The precursors, whose composition corresponds to the formula $0.97ZrO_2{\cdot}0.03Y_2O_3$, were synthesized by the precipitation of

* Corresponding author. Tel./fax: +380 44 4242211.
E-mail address: krawtschyk@yahoo.com (K.V. Kravchyk).

0022-3093/$ - see front matter Crown Copyright © 2009 Published by Elsevier B.V. All rights reserved.
doi:10.1016/j.jnoncrysol.2009.09.012

hydroxides (sequential precipitation (I) and coprecipitation (II)) of appropriate metals and by sol–gel method (III).

To synthesize samples I and II, 2 M aqueous solutions of $ZrOCl_2$ and $Y(NO_3)_3$ were used as starting salts. $ZrO(OH)_2$ and $Y(OH)_3$ were precipitated with concentrated aqueous solution of ammonia. In the case I, $Y(OH)_3$ was precipitated on precipitated $ZrO(OH)_2$, and in the case II, the hydroxides $ZrO(OH)_2$ and $Y(OH)_3$ were coprecipitated. The precipitates were washed free from the mother solution with distilled water until there were no Cl^- and NO_3^- ions in the washings. The filtration coefficient (K_f) of freshly precipitated precipitates was determined by the procedure described in [19].

To prepare precursors by the sol–gel method, alcoholic solutions of zirconium oxochloride $ZrOCl_2$ and yttrium nitrate $Y(NO_3)_3$ were used. The solutions were prepared on the basis of 96% ethyl alcohol with an overall concentration of salts in alcohol in terms of oxides of 0.4 mol/l. After 2 weeks of holding in a closed vessel, the alcoholic gel formed was dried at room temperature until xerogel was formed.

Air-dry xerogels and xerogels calcined at $T = 870$ K/1 h were investigated, which had been prepared by sequential precipitation and coprecipitation of hydroxides and by the sol–gel method (samples I, II, III).

Thermal analysis (TGA) was performed with a Setaram TGDTA92 equipment at a heating rate of 5 °C min^{-1} in air using Pt crucibles. The measurement error of the water content in precipitates was ±0.1%.

X-ray diffraction (XRD) measurements were made on a DRON 4-07 powder diffractometer (CoKα radiation, 40 kV, 18 mA). The structure parameters were calculated by the Rietveld full-profile analysis. XRD patterns were collected in the angular range $2\theta = 10°$–$150°$ in a step-scan mode with a step size $\Delta 2\theta = 0.02°$ and a counting time of 10 s per data point. As external standards, we used SiO_2 (2θ calibration) and Al_2O_3 (intensity standard) [20]. The size of coherently scattering domains (CSDs) and lattice strain were evaluated from the width of the 101 and 202 diffraction peaks using the relation $\beta\cos\theta = f(\sin\theta) = \lambda/D + 2\eta\sin\theta$ [21], where β is the peak width at half maximum, λ is the X-ray wavelength, and η is the lattice strain. Peak width at half maximum and its error were determined by using Gaussian equation (Origin 7.5 program). The error of determination of size of CSDs was ±0.2 nm.

The mechanical strength (Pm) of xerogel and oxide agglomerates was determined by commonly used method from the maximum force of crushing of granules between two hard supports [22]. The measurement error of the mechanical strength of agglomerates was ±0.1 MPa.

The densities samples were measured by Archimedes method. Density measurements were repeated three to four times per sample and were done with a precision of better than 0.1%, the maximum error was in the range of ±0.01 to 0.03 g/cm^3.

Small-angle X-ray scattering (SAXS) curves were measured in a vacuum Kratky camera using a Cu-anode tube as the X-ray source. The radiation was monochromatized by total internal reflection and a nickel filter [23]. SAXS data were collected in multiple step-scan mode, using a scintillation detector, at scattering angles from 0.03° to 4.0° ($q = 4\pi\sin\theta/\lambda = 0.022 - 2.86\ nm^{-1}$), which allowed characterization of microinhomogeneities 2–380 nm in size (determined as $2\pi/q$). The SAXS data were processed with the FFSAXS program [23,24] to eliminate the stray scattering by the camera and cuvette windows, normalize the scattered intensity to absolute units, and introduce the collimation correction. The fine powders to be studied were placed in cuvettes 0.1–0.2 mm in thickness, with 17-μm-thick Mylar windows.

To analyze SAXS profiles, we used Beaucage's unified exponential/power-law approach [25–28]. The equation describing an arbitrary number of interrelated structural levels has the form

$$I(q) = \sum_{i=1}^{n} \left(G_i \exp(-q^2 R_{g_i}^2/3) + B_i \exp(-q^2 R_{g_{(i+1)}}^2/3) \times \left\{ \left[erf(qR_{g_i}/6^{1/2}) \right]^3 / q \right\}^{-P_i} \right), \quad (1)$$

where G_i is the Guinier prefactor for level i, B_i is the Porod prefactor (in the power-law dependence of the logarithm of the scattered intensity on the logarithm of the scattering vector), and P_i is the exponent defining the fractal dimension of aggregates at level i ($3 > P > 4$ for surface fractals and $1 > P > 3$ for mass fractals). The mass-fractal dimension is $D_m = P$, and the surface-fractal dimension is $D_s = 6 - P$. R_{g_i} is the radius of gyration of fractal aggregates at level i. The errors of determination of P_i and R_{g_i} have equated ±1% and ±0.5% accordingly.

3. Results

Table 1 presents a characterization of the samples of xerogels (I, II, III) and corresponding oxides under investigation. As is obvious from Table 1, the filtration coefficient (K_f) of precipitates I is by an order of magnitude higher than that of precipitates II, and the strength of aggregates of xerogels I (Pm) is lower by a factor of 50 than that of xerogels II. Calcined xerogels (870 K/1 h) I, II are characterized by single-phase fluorite-type cubic crystal structure (Fig. 1) with practically the same lattice parameters (Table 1) and xerogel III by tetragonal structure with the axial ratio $\bar{c}/a = 1.44$.

Fig. 2(a)–(c) shows SAXS curves for air-dry samples I, II, III respectively and Fig. 2(d)–(f) SAXS curves for the same samples after heat treatment at 870 K. The results of modeling of experimental data are listed in Table 2. It is seen from Fig. 2(a) and (b) that the curves are characterized by three (for hydroxide samples I and II) and two (for sol–gel samples III) linear regions (straight-line segments), over which the corresponding slope angle values are given. The type of fractal aggregation for each region and fractal dimension was determined from the slope angle of such regions.

Mass (bulk) and surface fractals are the simplest and commonest types of fractal aggregation in disperse systems [8].

From the result presented (Fig. 2(a) and (b)) and Table 2) it is obvious that xerogels I and II are characterized at the first lowest

Table 1
Characterization of the samples under investigation, obtained under different synthesis conditions.

Samples	Xerogels $0.97ZrO(OH)_2 \cdot 0.06Y(OH)_3$				Powders $0.97ZrO_2 \cdot 0.03Y_2O_3$			Pills $0.97ZrO_2\ 0.03Y_2O_3$
	K_f (cm/s)	H_2O (total) (%)	H_2O(v) (%)	Pm (MPa)	Grain size D (nm) (SAXS)	CSR size (nm)	Lattice parameters (Å)	Green density (g/cm^3)
SPH (I)	$5.6 \times 10^{-5} \pm 0.1 \times 10^{-5}$	34.6 ± 0.1	0.5 ± 0.1	0.4 ± 0.1	12.0 ± 0.5	13.0 ± 0.2	$a = 5.1195 \pm 1 \times 10^{-4}$	2.00 ± 0.01
CPH (II)	$5.2 \cdot 10^{-6} \pm 0.2 \times 10^{-6}$	36.3 ± 0.1	1.5 ± 0.1	20.0 ± 0.1	11.0 ± 0.4	9.0 ± 0.2	$a = 5.1197 \pm 1 \times 10^{-4}$	2.42 ± 0.03
Sol–gel (III)	–	–	–	18.0 ± 0.1	18.0 ± 0.4	17.0 ± 0.2	$a = 3.6031 \pm 2 \times 10^{-4}$ $c = 5.1807 \pm 2 \times 10^{-4}$	2.97 ± 0.02

Note: H_2O(v) is the content of the water that vaporized during crystallization, Pm is mechanical strength of agglomerates.

Please cite this article in press as: K.V. Kravchyk et al., J. Non-Cryst. Solids (2009), doi:10.1016/j.jnoncrysol.2009.09.012

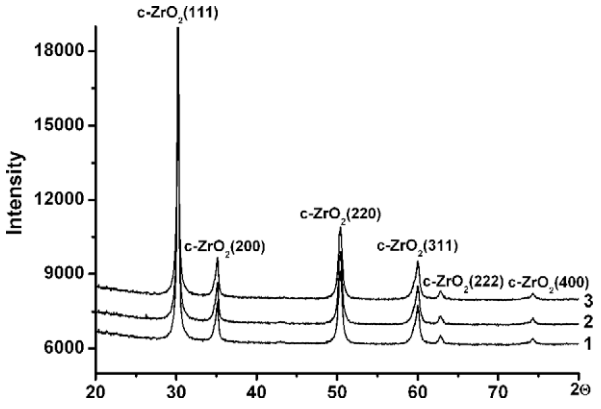

Fig. 1. Diffractograms of calcined samples at $T = 870$ K/1 h: (1) sample I; (2) sample II, (3) samples III.

aggregation level (the range of maximum q values and hence minimum values of dimensions) by the presence of mass fractals (primary particles of fractal object) with the radii of rotation $R_g = 3.0$ and 2.5 nm and fractal dimension $D = 1.1$ and 1.5 respectively. This corresponds to the formation, at the first dimensional level, of oblong particles with a mean diameter of $d = 7.7$ nm and 6.5 respectively. The increase in the fractal dimensions, at this level, of samples II in comparison with that of samples I indicates that the particles obtained under the conditions II are more bulky [8]. This may be attributed to their higher water content [29]. The change in the slope of SAXS curves (Fig. 2(a) and (b)) and the increase in fractal dimension are associated with the aggregatability of primary particles into surface fractals of larger size ($d = 77.4$ nm for I and 56.8 nm for II). Surface fractals form at a higher (third) structure level mass fractals for samples I and surface fractals for samples II with a mean diameter of $d = 335$ nm and 387 nm respectively.

Xerogels III are characterized, at the initial stage of aggregation, by the presence of surface-fractal particles ($D = 2.75$) with a mean diameter (d_s) of 23 nm (Fig. 2(c)). At the second stage of aggregation, surface fractals ($D = 2.25$) with the diameter $d_s \geqslant 258$ nm are also formed.

As is seen from Fig. 2(d)–(f), the SAXS curves for calcined xerogels are characterized, independent of precursor preparation con-

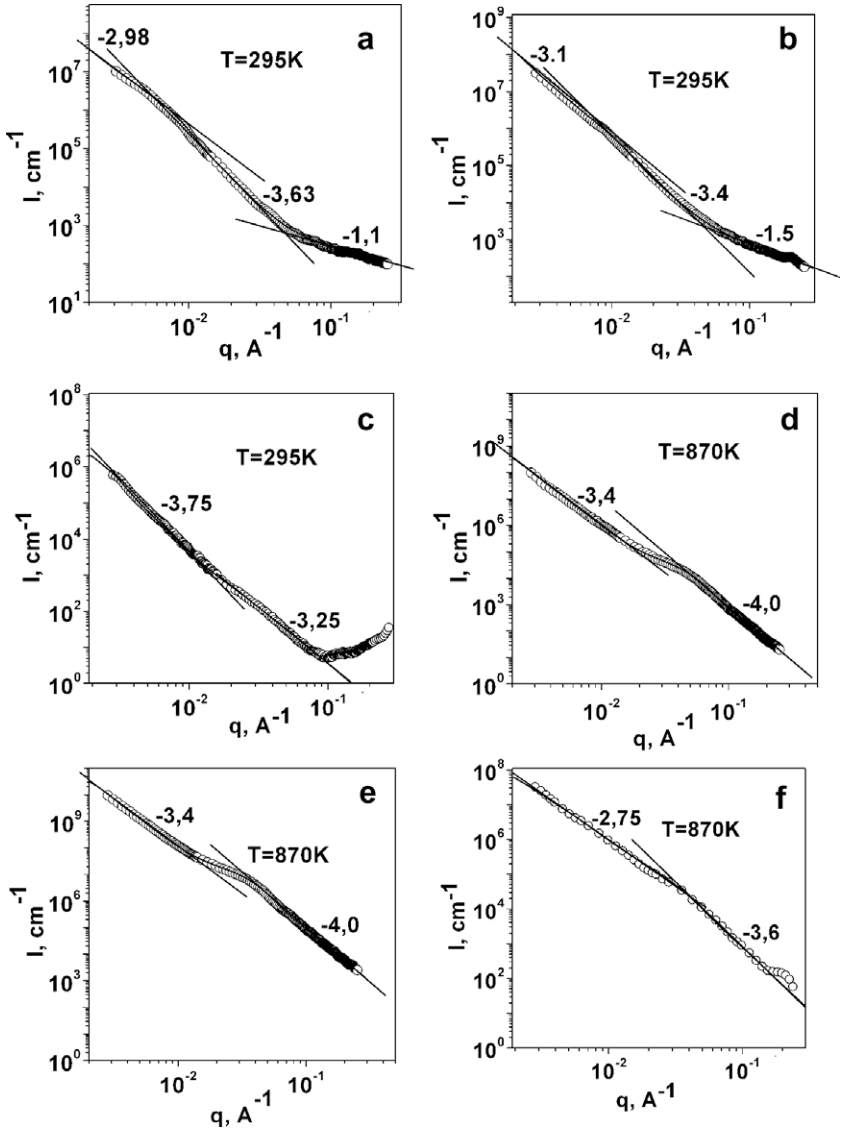

Fig. 2. Small-angle X-ray scattering curves for air-dry samples I (a), II (b) and III (c) ($T = 295$ K) and calcined samples I (d), II (e) and III (f) ($T = 870$ K): I is intensity; q is wave vector. The linear regions of small-angle X-ray scattering curves are presented by imaginary straight-line segments. The corresponding slope angle values calculated by fitting of SAXS curves by using the Beaucage's equation [25–28] are given over the linear regions.

Please cite this article in press as: K.V. Kravchyk et al., J. Non-Cryst. Solids (2009), doi:10.1016/j.jnoncrysol.2009.09.012

Table 2
Structural parameters determined by fitting the SAXS curves of xerogels and powders with unified functions.

Sample	Structural level	Fractal type	s	D	R_g (нм)	d_s (нм)
SPH (I) T = 295 K	1	M	−1.10	1.1	3.0	7.7
	2	S	−3.63	2.37	30	77.4
	3	M	−2.8	2.8	130	335
CPH (II) T = 295 K	1	M	−1.5	1.5	2.5	6.5
	2	S	−3.4	2.6	22	56.8
	3	S	−3.3	2.7	150	387
Sol–gel method (III) T = 295 K	1	S	−3.25	2.75	9.0	23
	2	S	−3.75	2.25	⩾100	⩾258
SPH (I) T = 870 K	1	S	−4	2	4.5	12
	2	S	−3.4	2.6	120	310
CPH (II) T = 870 K	1	S	−4	2	6.0	11
	2	S	−3.4	2.6	120	310
Sol–gel method (III) T = 870 K	1	S	−3.6	2.4	7.0	18
	2	M	−2.75	2.75	⩾100	⩾258

Note: M = mass fractal, S = surface fractal, s is the power-law slope in the SAXS curve, D is the fractal dimension, R_g is the radius of gyration of fractal aggregates, and $d_s = 2.58 * R_g$. The errors of determination of the power-law slopes (s) in the SAXS curves and of the radiuses of gyration of fractal aggregates (R_g) are ≈±1 and ±0.5% accordingly.

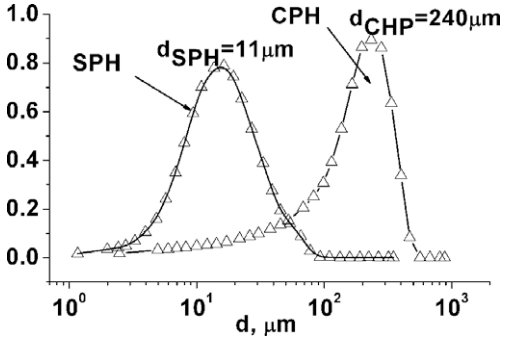

Fig. 3. Size distribution curves for sequentially precipitated and co-precipitated aggregated hydroxides after calcination at 870 K.

ditions, by two linear regions, indicating the presence of a two-level fractal structure in the calcined powders. At the first structure level, surface fractals of 11.6, 15.5 and 18 nm size are formed for samples I, II and III respectively. The values of fractal dimensions are 2 for samples I and II and 2.4 for samples III. This indicates that the shape of the first-level aggregates is close to spherical one. The surface of samples I and II may be characterized as smooth and that of samples III as surface with feebly marked roughness. At the second structure level, particles of samples I and II aggregate (the slope of SAXS curves changes greatly), forming surface fractals of the same size (d = 310 nm) with rough, branched surface (see Table 2; $D \to 3$). Particles of samples III aggregate into mass fractals with the mean diameter $d_s \geqslant 258$ nm (see Table 2).

4. Discussion

The sequence of the fractal aggregation types of xerogels (starting from the lowest level) is as follows: $M \to S \to M$, $M \to S \to S$ and $S \to S$ for samples I, II and III respectively. The difference in the methods for the preparation of precursors (precipitation hydroxides from aqueous solutions and sol–gel in alcohol-aqueous solutions) tells on the number of fractal aggregation levels of xerogels (see Fig. 2(a)–(c)), Table 2). For instance, for hydroxide xerogels (I, II) three-level fractal structures and for sol–gel samples (III) two-level fractal structures are observed. It is evident that this difference is associated with a difference in the coagulation kinetics of hydroxide sols (I, II) and polymeric organic–inorganic zirconium complexes (III), which depend on the nature of the dispersion medium, disperse phase concentration, salvation shell, double electrical layer, etc. In the sol–gel technology, in comparison with precipitation of hydroxides from aqueous solutions, there is slow sol coagulation due to the use of dilute stock solutions, particle surface passivation by hydrocarbon radicals, and limitation of particle diffusion caused by the viscosity of alcoholic sol. The type of coagulation (fast, slow) has an effect on the fractal dimension of aggregates [30]. The fractal dimension of aggregates obtained under slow coagulation conditions is larger than that of aggregates obtained under fast coagulation conditions [30]. This is observed for xerogel clusters at the first structure level (see Table 2; D = 2.75 for sample III, D = 1.1 and 1.5 for samples I and II). The larger fractal dimension of xerogels III indicates higher organization of nanoparticles in sol–gel clusters as against zirconium hydroxide clusters [30]. The effect of hydroxide precipitation conditions (I and II) on the type of fractal aggregation manifests itself at the third structure level. In the case coprecipitation (II), surface-fractal agglomerates with rough surface (D = 2.7) are formed at the third structure level instead of mass-fractal agglomerates, which are characteristic of sequential precipitation of hydroxides (I). In this case, the size of agglomerates increases by a factor of 1.15. Taking into account the difference in the structure of mass and surface fractals [8], it becomes understandable why the filtration coefficient of samples I is by an order of magnitude larger than that of samples II (Table 1). During filtration through a hydroxide precipitate with surface-fractal aggregation, water will easily pass through the surface layer and be retained in the bulk. The precipitates with mass-fractal aggregation have a loose structure in the whole volume, therefore water passes easily through the precipitate layer at a high rate. The adverse effect of the degree of hydration of precipitates on their filterability should also be taken into account. The higher water content of precipitates II as against precipitates I (Table 1) makes for poorer filterability [29]. It should be noted that xerogels I are characterized by weak bonds between particles in comparison with xerogels II. This manifest itself by the friability of the former (aggregates of particles I easy broken up on light pressure on them, whereas a certain force is required to crush aggregates II (Table 1)).

The sequence of the fractal aggregation types of calcined xerogels (solid solutions of $0.97ZrO_2 \cdot 0.03Y_2O_3$ oxides) I and II is $S \to S$ and for samples III $S \to M$ (Table 2). During the thermal decomposition of air-dry samples I, II and III at 670–870 K, a labile active reaction medium begins to form, in which nanoclusters of zirconium and yttrium oxides are generated. Their interaction in a solid is determined by diffusion limitation (cluster growth is limited by the distance which depends on the diffusion coefficient of metals)

Please cite this article in press as: K.V. Kravchyk et al., J. Non-Cryst. Solids (2009), doi:10.1016/j.jnoncrysol.2009.09.012

[30]. It follows from comparison of fractal parameters (number of levels and fractal size) of xerogels and calcined samples I and II that when xerogels are heat-treated at 870 K, there is a weak interaction between the clusters of the first structure level. This result in the formation of two-level fractal structure of initial precipitates of $0.97ZrO_2{\cdot}0.03Y_2O_3$ oxides.

It is evident from the above result that the crystal structure (Fig. 1, Table 1) and the structure parameters of calcined samples I and II (Fig. 2(d) and (e)), Table 2) are identical. However, samples I and II (as well as corresponding xerogels) differ widely in the strength of aggregates (agglomerates) (Table 1). This is corroborated by distribution curves for aggregated particles of samples I and II after calcinations at 870 K (Fig. 3). As is seen from Fig. 3 and 80–90% conglomerates of particles of samples I and II formed at a higher structure level is characterized by a mean size of d = 11 μm and d = 240 μm respectively. Agglomerates I with weaker bonds between particles are readily broken by ultrasound to a lower dimensional level. It is obvious that the difference in the strength of aggregates of oxides is associated with the difference in the fractal types of precursors (hydroxides). It is known [7] that the nanostructures of the first structure level are 'bricks' of which hierarchic nanostructures are made up at higher dimensional levels (aggregate–agglomerate–conglomerate) (Fig. 3). Such 'bricks' for precursors I and II are mass-fractal nanostructures (Table 2). The difference between the nanostructures of xerogels I and II manifests itself at the third structure level. As follows from the results presented (Table 2), the ratio of the numbers of the levels of fractal types, M: S, in the order I, II, III is 2: 1, 1: 2, 0: 2 respectively. The weak bonds between the particles of the end product ($0.97ZrO_2{\cdot}0.03Y_2O_3$) may be due to the larger content of mass (loose) fractals of xerogels. In this case, both the pressability of oxide powders and the green density of pressed samples decreases. Otherwise, the pressability increases with increasing of the content of surface (denser) fractals (see Table 1 and 2). Thus, the self-assembly of particles in precursors determines the technological properties of ZrO_2-based oxides. There results demonstrate clearly the manifestation of the effect of topochemical memory [5].

As follows from Table 1, the mean particle size at the first structure level of calcined samples I, II and III (d_{SPH} = 12 nm, d_{CPH} = 11 nm, $d_{sol-gel}$ = 18 nm) agrees with the size of the coherent-scattering region (CSP) (d_{SPH} = 13 nm, d_{CPH} = 9 nm, $d_{sol-gel}$ = 17 nm). Thus the results obtained by the SAXS method and wide-angle X-ray diffraction showed a good agreement, which confirms the results obtained to be reliable and the investigation of disperse systems by the SAXS method to be worth-while.

5. Conclusions

The effect of the method for the preparation of the precursor of yttrium-stabilized zirconium dioxide (precipitation of hydroxides from aqueous solutions and sol–gel from alcoholic solutions) and the conditions of preparation of hydroxides (sequential precipitation and coprecipitation) on the fractal structure of xerogels and oxides with fluorite structure has been studied.

It has been shown that the difference of the methods manifests itself clearly in xerogel nanostructures, viz. by the number of fractal aggregation levels (three levels in hydroxide precipitates and two in sol–gel) and the absence of mass-fractal aggregation in sol–gel. The difference in the conditions of preparation of hydroxides manifests itself by the sequence of fractal types.

The correlation: nature of precursor – type of fractal aggregation – technological properties of ZrO_2 powders has been established. It is been shown that the mass-fractal aggregation of precursors contributes to good filtration of hydroxide precipitates and allows preparation of oxides with soft, readily destructible aggregates, and that surface-fractal aggregation makes for good pressability of oxides.

References

[1] D. Marshall, J.J. Ratto, F.F. Lunge, J. Am. Ceram. Soc. 74 (1991) 2979.
[2] G. Chiodelli, G. Flor, M. Scagliotti, Solid State Ion. 91 (1996) 109.
[3] J.H. Lee, J. Kim, S.W. Kim, H.W. Lee, H.S. Song, Solid State Ion. 166 (2004) 45.
[4] K. Kawamura, K. Watanabe, T. Hiramatsu, A. Kaimai, Y. Nigara, T. Kawada, J. Mizusaki, Solid State Ion. 144 (2001) 11.
[5] Yu.D. Tretyakov, Russ. Chem. Rev. 72 (2003) 651.
[6] V.I. Roldughin, Russ. Chem. Rev. 73 (2004) 115.
[7] A.P. Shpak, P.G. Cheremskoi, Yu.A. Kunitskii, O.V. Sobol, Klasternye i nanostructurnye materially, Kiev, 2005, Part 3, p. 142.
[8] A.P. Shpak, V.V. Shilov, O.A. Shilova, Yu.A. Kunitskii, Diagnostika nanosistem, Mnogourovnevye fraktal'nye nanostruktury (Evaluation of Nanosystems: Multilevel Fractal Nanostructures), Kiev, 2004, Part 2, p. 111.
[9] J. Feder, Fractals, Plenum, New York, 1988, Translated under the title Fraktaly, Mir, Moscow, 1991, p. 19.
[10] G.N. Fedotov, Yu.D. Tret'yakov, E.I. Pakhomov, A.I. Kuklin, A.Kh. Islamov, Dokl. Chem. 407 (2006) 51.
[11] G.N. Fedotov, Yu.D. Tret'yakov, V.K. Ivanov, A.I. Kuklin, A.Kh. Islamov, V.I. Putlyaev, A.V. Garshev, E.I. Pakhomov, Dokl. Chem. 404 (2005) 638.
[12] S.V. Kalinin, D.L. Gorbachev, A.Yu. Borisevich, K.V. Tomashevitch, A.A. Vertegel, A.J. Markworth, Yu.D. Tretyakov, Phys. Rev. 61 (2000) 1189.
[13] S.V. Kalinin, A.A. Vertegel, N.N. Oleynikov, Yu.D. Tretyakov, J. Mater. Syn. Process. 6 (1998) 305.
[14] V.Ya. Shur, S.A. Negashev, A.L. Subbotin, et al., Fiz. Tverd. Tela (S.-Peterburg) 41 (1999) 306.
[15] V.Ya. Shur, G.G. Lomakin, V.P. Kuminov, et al., Fiz. Tverd. Tela (S.-Peterburg) 41 (1999) 306.
[16] Y. Zeng, Y. Zhao, J. Colloid Interface Sci. 247 (2002) 100.
[17] Y.W. Zeng, P. Riello, A. Benedetti, G. Fagherazzi, J. Non-Cryst. Solids 185 (1995) 78.
[18] O. Stachs, Th. Gerber, Y. Beyer, H. Biirger, J. Non-Cryst. Solids 180 (1995) 197.
[19] I.M. Vaserman, Khimicheskoe osazhdenie iz rastvorov (Chemical Precipitation from Solutions), Leningrad, Khimiya, 1980, p. 16.
[20] Certificate of Analysis: Standard Reference Material 1976, Instrument Sensitivity Standard for X-Ray Powder Diffraction, Natl. Inst. of Standards and Technology, Gaithersburg, 1991. p. 1.
[21] H. Ohsato, M. Imaeda, Y. Takagi, in: Proceedings of the Eleventh IEEE International Symposium on Applications of Ferroelectrics, Mountrex, August 24–27, 1998. p. 509.
[22] V. Dubok, M. Kabanova, N. Pavlenko, Powder Metall. 12 (1988) 18.
[23] C.G.Vonk, FFSAXS's Program for the Processing of Small-Angle X-ray Scattering Data, Geleen, DSM, 1974, p. 83.
[24] Yu.S. Lipatov, V.V. Shilov, Yu.P. Gomza, R.S. Kruglyak, Rentgenograficheskie metody izucheniya polimernykh sistem (X-ray Diffraction Characterization of Polymer Systems), Kiev, Naukova Dumka, 1982, p. 29.
[25] G. Beaucage, J. Appl. Crystallogr. 28 (1995) 717.
[26] G. Beaucage, J. Appl. Crystallogr. 29 (1996) 134.
[27] J. Hyeon-Lee, G. Beaucage, S.E. Prausnits, S. Vemury, Langmuir 14 (1998) 5751.
[28] O.A. Shilov, V.V. Shilov, Nanosist., Nanomater., Nanotekhnol. 1 (2003) 9.
[29] A.G. Belous, E.V. Pashkova, A.N. Makarenko, et al., Inorg. Mater. 33 (1997) 1246.
[30] I.P. Suzdalev, P.I. Suzdalev, Russ. Chem. Rev. 75 (2006) 637.

Please cite this article in press as: K.V. Kravchyk et al., J. Non-Cryst. Solids (2009), doi:10.1016/j.jnoncrysol.2009.09.012